

Journal Pre-proof

Steering CO₂ electrolysis selectivity by modulating the local reaction environment: an online DEMS approach for Cu electrodes

Ke Ye, Guiru Zhang, Baoxin Ni, Liang Guo, Chengwei Deng, Xiaodong Zhuang, Changying Zhao, Wen-Bin Cai, Kun Jiang

PII: S2667-1417(23)00068-X

DOI: <https://doi.org/10.1016/j.esci.2023.100143>

Reference: ESCI 100143

To appear in: *eScience*

Received Date: 28 February 2023

Revised Date: 31 March 2023

Accepted Date: 16 May 2023

Please cite this article as: K. Ye, G. Zhang, B. Ni, L. Guo, C. Deng, X. Zhuang, C. Zhao, W.-B. Cai, K. Jiang, Steering CO₂ electrolysis selectivity by modulating the local reaction environment: an online DEMS approach for Cu electrodes, *eScience*, <https://doi.org/10.1016/j.esci.2023.100143>.

This is a PDF file of an article that has undergone enhancements after acceptance, such as the addition of a cover page and metadata, and formatting for readability, but it is not yet the definitive version of record. This version will undergo additional copyediting, typesetting and review before it is published in its final form, but we are providing this version to give early visibility of the article. Please note that, during the production process, errors may be discovered which could affect the content, and all legal disclaimers that apply to the journal pertain.

© 2023 The Authors. Published by Elsevier B.V. on behalf of Nankai University.



Steering CO₂ electrolysis selectivity by modulating the local reaction environment: an online DEMS approach for Cu electrodes

Ke Ye,¹ Guiru Zhang,¹ Baoxin Ni,¹ Liang Guo,² Chengwei Deng,³ Xiaodong Zhuang,⁴
Changying Zhao,² Wen-Bin Cai,⁵ Kun Jiang^{1,2*}

¹ Interdisciplinary Research Center, School of Mechanical Engineering, Shanghai Jiao Tong University, Shanghai 200240, China.

² China-UK Low Carbon College, Shanghai Jiao Tong University, Shanghai 201306, China.

³ State Key Laboratory of Space Power-Sources Technology, Shanghai Institute of Space Power Sources, Shanghai 200245, China.

⁴ School of Chemistry and Chemical Engineering, Frontiers Science Center for Transformative Molecules, Shanghai Jiao Tong University, Shanghai 200240, China.

⁵ Shanghai Key Laboratory of Molecular Catalysis and Innovative Materials, Collaborative Innovation Center of Chemistry for Energy Materials, Department of Chemistry, Fudan University, Shanghai 200438, China.

* To whom correspondence should be addressed: K.J. (Email: kunjiang@sjtu.edu.cn)

Abstract

Electrochemical CO₂ reduction is a typical surface-mediated reaction, with its reaction kinetics and product distributions largely dependent on the dynamic evolution of reactive species at the cathode–catholyte interface and on the resultant mass transport within the hydrodynamic boundary layer in the vicinity of the cathode. To resolve the complex local reaction environment of branching CO₂ reduction pathways, we here present a differential electrochemical mass spectroscopic (DEMS) approach for Cu electrodes to investigate CO₂ mass transport, the local concentration gradients of buffering anions, and the Cu surface topology effects on CO₂ electrolysis selectivity at a temporal resolution of ~400 ms. As a proof of concept, these tuning knobs were validated on an anion exchange membrane electrolyzer, which delivered a Faradaic efficiency of up to 40.4% and a partial current density of 121 mA cm⁻² for CO₂-to-C₂H₄ valorization. This methodology, which bridges the study of fundamental surface electrochemistry and the upgrading of practical electrolyzer performance, could be of general interest in helping to achieve a sustainable circular carbon economy.

Keywords

Spectroelectrochemistry; CO₂ reduction reaction; Copper electrode; Differential electrochemical mass spectroscopy; Local reaction environment

Introduction

With dwindling fossil fuels and rising concerns about anthropogenic global warming, the electrochemical CO₂ reduction reaction (CO₂RR) has attracted considerable interest in recent decades as a means toward transitioning from a linear to a circular carbon economy, as well as for the distributed storage of intermittent renewable energies in the meantime [1-5]. Of the CO₂RR catalysts explored so far, Cu is the sole monometallic candidate capable of valorizing CO₂ into C₂₊ products with high Faradaic efficiency (FE) [6]. However, the process is still challenged by diverse product distributions and slow reaction kinetics arising from the multiple proton-coupled electron transfer steps [7], as well as strong competition from the side hydrogen evolution reaction (HER) [8].

To address these issues, extensive efforts have been carried out to improve the intrinsic C–C coupling performance over Cu catalysts, including but not limited to preferential facet exposure [9-12], surface topology and defects engineering [13-15], and alien component alloying [16-20]. Extrinsicly, tailoring the microenvironment near the electrode holds the potential to increase activity and selectivity; various methods include coating ionomers and modifiers on Cu surfaces [21-23], optimizing the concentrations of cations and anion in electrolytes [24-27], enhancing mesoscale mass transport [28, 29], and adjusting local CO pressure/coverage [30, 31].

It should be noted that since the CO₂RR is a typical surface-mediated reaction, the complex local reaction environment plays a vital role in defining the reaction performance; this can involve the Cu catalyst's structure, the cathode–catholyte interface, plus the aforementioned dynamic boundary layer conditions in the vicinity of the cathode [32-34]. Alongside the search for more active and selective CO₂RR catalysts, work in recent years has indicated the need to shed light on the complicated CO₂RR reaction mechanism at the molecular level and to probe how the dynamic local reaction environment affects the branching of CO₂RR product distributions in real time. In addition to conventional headspace gas chromatography (GC) and *ex situ* ¹H nuclear magnetic resonance (NMR) quantification methods, recent advances of *in situ* spectroelectrochemistry, such as vibrational [35, 36] and synchrotron radiated spectroscopies [37, 38], have helped resolve the dynamic evolution of catalyst structure and local environment during CO₂RR at the molecular level. For instance, by deploying shell-isolated nanoparticle-

enhanced Raman spectroscopy, Li et al. successfully captured key CO₂RR intermediates of *CO, *COOH, *OCCO, and *CH₂CHO over a series of Cu(*hkl*) single-crystal electrodes, further correlating *CO coverage with C₂ product selectivity over different Cu model surfaces [39].

Differential electrochemical mass spectroscopy (DEMS) is another powerful tool for directly correlating the apparent electrocatalytic performance with the local reaction environment [40, 41]. In 2006, Koper *et al.* came up with a probe-inlet online electrochemical mass spectrometry system by placing a Peek holder covered with porous Teflon membrane in close proximity (ca. 10–20 μm) to the electrode surface. The reaction rate of certain reactants and products could thus be tracked at a temporal resolution of seconds by recording relevant mass ion signals, and this apparatus was successfully adapted for the electrooxidation of small fuel molecules [42, 43] and the Cu-catalyzed CO₂RR [44]. To eliminate the retardation time between Faradaic and mass ion currents, as well as to mitigate potential disturbance of the reaction microenvironment by the inlet probe, Bell *et al.* developed a membrane-inlet DEMS flow cell with a catalyst cast porous PTFE film; this served as both the pervaporation membrane and the working electrode. A precedence relation between C₂₊ aldehydes and alcohols in the immediate vicinity of the cathode surface was revealed [45], reinforced by follow-up aldehyde co-electrolysis experiments using a similar DEMS approach [46] and by proton transfer reaction time-of-flight mass spectroscopic measurements [47].

Here, we report the merits of investigating the local reaction environment effect on the Cu-catalyzed CO₂RR via a synergetic approach combining online DEMS with numerical simulations. The tuning knobs are CO₂ mass transport, the local concentration gradients of buffering anions, and the Cu surface topology, which have been screened at a temporal resolution of ~400 ms. Hints from this fundamental spectroelectrochemical study have been further validated in an anion exchange membrane electrolyzer, fulfilling a feedback loop between surface electrochemistry and pilot device performance upgrading.

Results and Discussion

CO₂ mass transport effect

A spectroelectrochemical flow cell design with well-defined mass transport (Fig. S1) [48]

allowed the real-time visualization of CO₂ depletion/utilization by online DEMS, in which a direct membrane-inlet configuration was deployed to improve the detection efficiency of a quadrupole mass spectrometer [45]. A microporous PTFE film coated with a ca. 300 nm Cu catalyst layer was used for pervaporation, separating the spectroelectrochemical cell from the vacuum system and facing the catholyte flow as the working electrode.

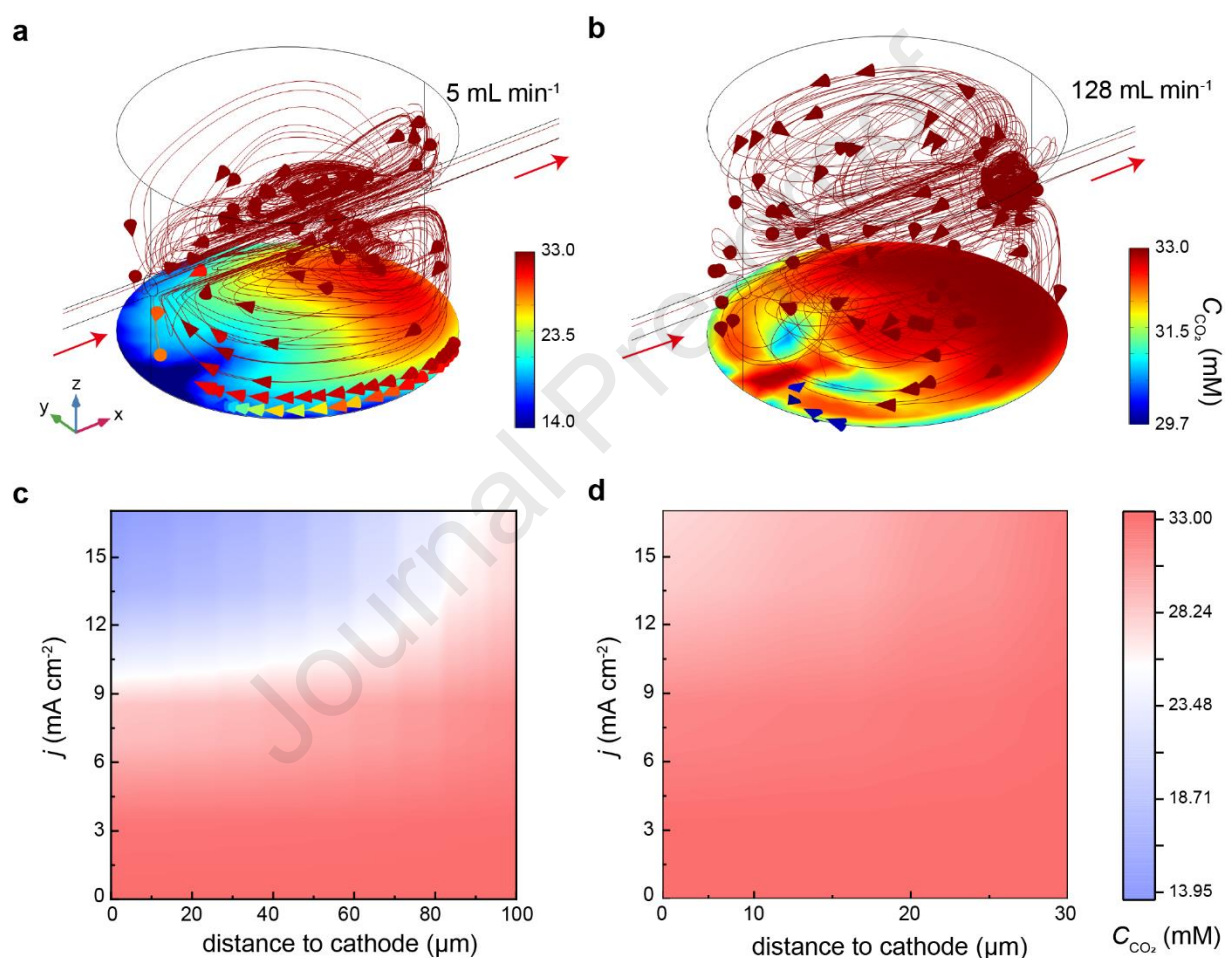


Fig. 1. Simulation CO₂ streamline within the customized DEMS cell at an inlet catholyte flow rate of (a) 5 mL min⁻¹ and (b) 128 mL min⁻¹, with a given current density of 7.0 mA cm⁻². The CO₂ consumption rate was calculated based on relevant CO₂RR product distributions as adopted from Jaramillo's work [49]. (c, d) Corresponding CO₂ concentration profile as a function of current density and distance to the cathode. The arrows in panels (a, b) indicate the direction of catholyte flow. The integrated spectroelectrochemical cell setup can be seen in Fig. S1.

Figs. 1a and 1b depict the simulated CO₂ streamline in the cathodic chamber at different

inlet flow rates of 0.1 M CO₂-saturated bicarbonate electrolyte but at the same current density of 7 mA cm⁻², using a three-dimensional computational fluid dynamics simulation in COMSOL Multiphysics. Representative CO₂RR product distributions as a function of applied potential and/or given current density were adopted from Jaramillo's seminal work (Table S1) [49]. A slow catholyte flow of 5 mL min⁻¹ was first simulated to approximate the static electrolysis in classic aqueous cells, with the CO₂ consumption rate ($R_{CO_2,con.}$) calculated as:

$$R_{CO_2,con.} = \sum \frac{j \times FE_i \times c_i}{n_i F} \quad (1)$$

where j is the total current density, and FE_i , c_i , and n_i are the Faradaic efficiency, carbon number, and electron transfer number of reduction product i , respectively. As shown in Fig. 1a, the CO₂ concentration in the vicinity of the cathode dramatically decreased from 33 mM in the bulk solution to ~14 mM, potentially restricting the CO₂RR current density and multi-carbon product selectivity. In the current flow cell design, this issue could be alleviated simply by increasing the inlet flow rate, i.e., tuning up to 128 mL min⁻¹ (the maximum rate delivered by our peristaltic pump, Fig. 1b). The consumed CO₂ reactant was replenished in a timely way due to efficient electrolyte circulation, maintaining a relatively high local CO₂ concentration above 30 mM. We further compared the mean CO₂ concentration profile along the z -axis as a function of the applied current density and the distance to the central point of the cathode, at an inlet catholyte flow rate of either 5 mL min⁻¹ (Fig. 1c) or 128 mL min⁻¹ (Fig. 1d); substantially enhanced CO₂ mass transport clearly resulted in the latter case, arising from the accelerated catholyte flow stream. Notably, the hydrodynamic boundary layer thickness was ca. 30 μm at 128 mL min⁻¹, in good agreement with a recent report on an aqueous flow-by cell [50] and much thinner than at 5 mL min⁻¹ (ca. 100 μm) in otherwise the same configuration.

Deconvolution protocol for DEMS signals

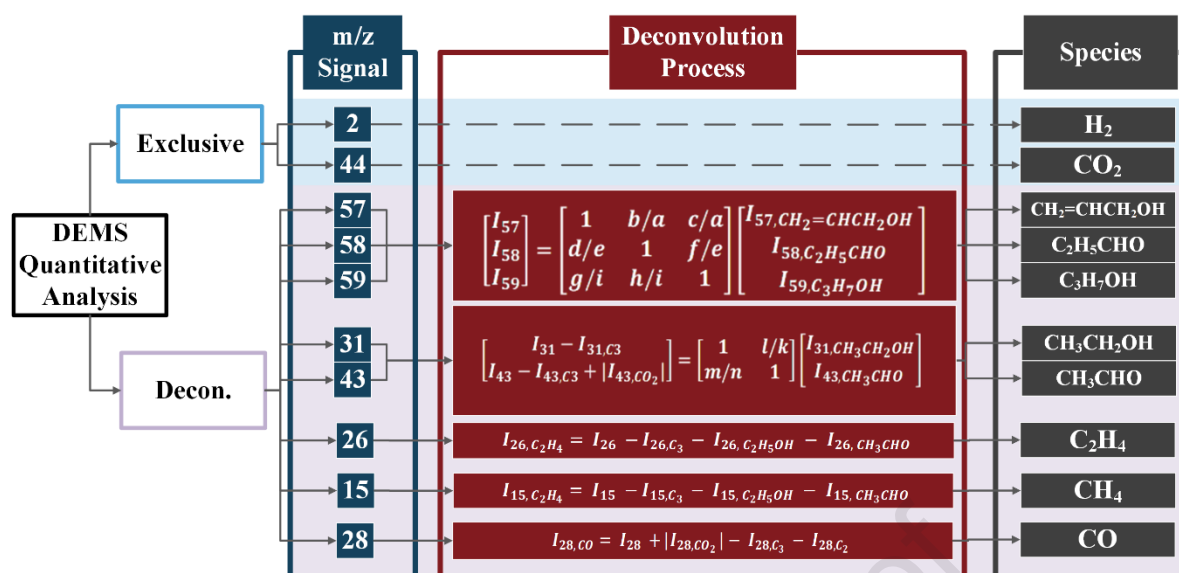


Fig. 2. Deconvolution protocol for DEMS signals over a typical Cu electrode during the CO₂RR, where I_x denotes the total signal intensity of $m/z = x$, and $I_{x,y}$ is the contributed signals from species y to overall I_x . The parameters $a, b, c, etc.$ denote the relative abundance of certain CO₂RR products as determined from their standard mass spectra, shown in Figs. S2 and S3; see also Table S8 for details.

Thereafter, the DEMS flow cell setup was deployed to investigate the effect of the local reaction environment on CO₂RR activity and selectivity over a polycrystalline Cu/PTFE film electrode as a stereotype. A variety of overlapped mass fragments were observed after electron ionization of different gaseous and volatile oxygenated products, thus calling for a cautious deconvolution step to probe the characteristic evolution dynamics for certain species. Fig. 2 demonstrates the protocol developed for m/z signal decoding, in which only H₂ and CO₂ generate exclusive fragments at $m/z = 2$ and 44, respectively, whereas all other CO₂RR products necessitate proper deconvolution to reflect their own dynamic concentration evolution near the cathode surface. Prior to DEMS measurements on Cu, we circulated standard aqueous samples containing each of certain 0.2 mol L⁻¹ C₂₊ oxygenates or C₂H₄-saturated 0.1 M CsHCO₃ in the cathodic chamber, then recorded each of their mass fragments and relative intensity distribution. As shown in Fig. S2, the determined mass spectra are roughly in agreement with those reported by different laboratories [45, 46] and the NIST database [51] (Tables S4–S7). Thereafter, the primary C₃ products allyl alcohol (CH₂=CHCH₂OH), propionaldehyde (C₂H₅CHO), and *n*-propanol (C₃H₇OH) could be preferentially analyzed due to their relatively large molecular weight, by taking into account the determined coefficients of peak intensity distribution for each

C_3 product to $m/z = 57, 58,$ and 59 in their standard mass spectra and solving the 3×3 matrix depicted in Fig. 2 (highlighted red region in the middle). Similarly, characteristic mass signals for the C_2 oxygenates C_2H_5OH ($m/z = 31$) and CH_3CHO ($m/z = 43$) could be deconvoluted in the same manner after subtracting the contributions from C_3 products (and the CO_2 contribution to $m/z = 43$, see Fig. S3). Compared to the assignable contributions from C_{2+} oxygenates to CH_4 at $m/z = 15$, their contribution to the mass signal of C_2H_4 ($m/z = 26$) is negligible, given their spectral intensity. CO is the last deconvoluted product, considering the overlapped contribution from CO_2 as well as other C_{2+} species to its characteristic mass-to-charge ratio of $m/z = 28$.

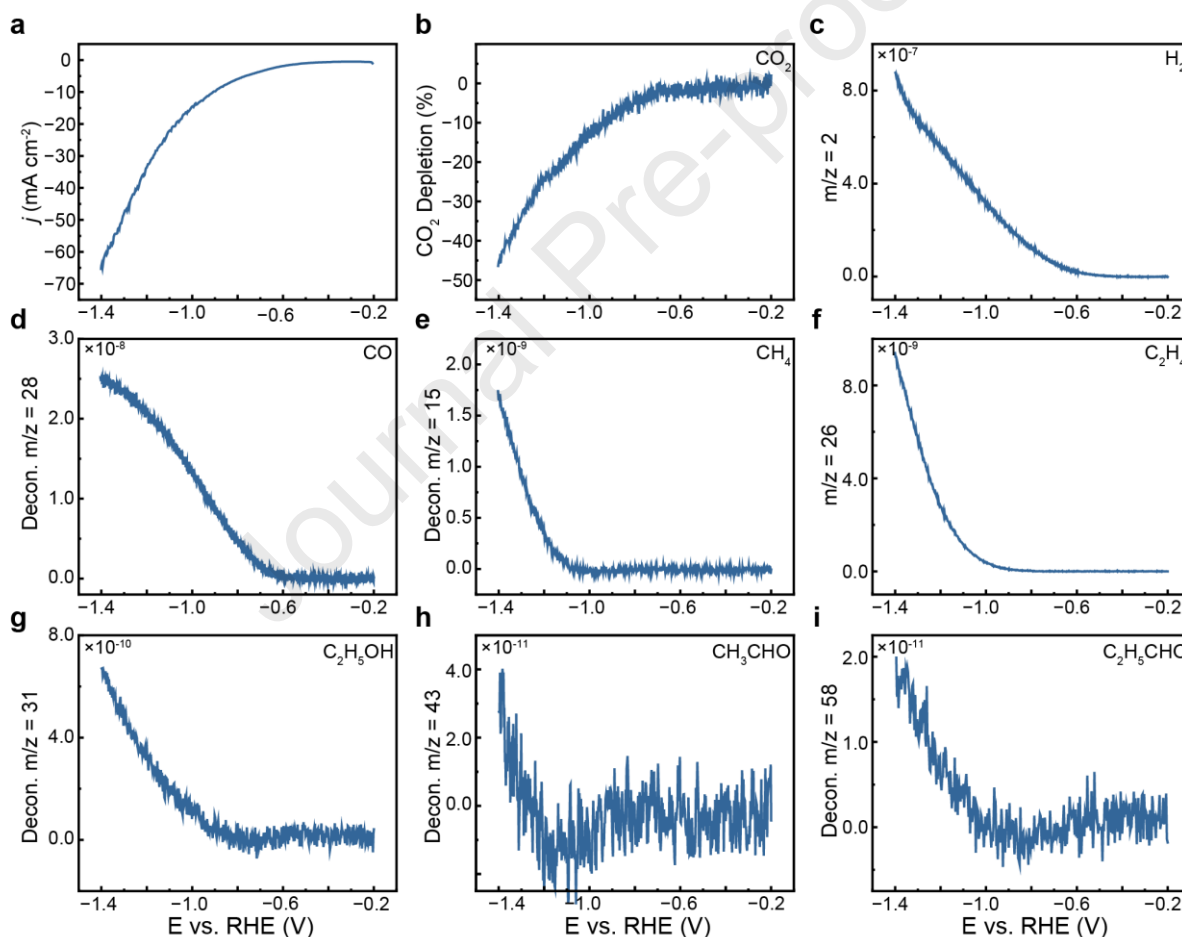


Fig. 3. Real-time DEMS results for the CO_2RR over a 300 nm sputtered Cu/PTFE electrode. (a) LSV recorded from -0.2 to -1.4 V vs. RHE at a scan rate of 5 mV s^{-1} in 0.1 M CsHCO_3 at a catholyte flow rate of 128 mL min^{-1} , together with the corresponding mass ion current plots of (b) CO_2 , (c) H_2 , (d) CO , (e) CH_4 , (f) C_2H_4 , (g) C_2H_5OH , (h) CH_3CHO , and (i) C_2H_5CHO . The other C_3 products $CH_2=CHCH_2OH$ and C_3H_7OH , at low production rates, are plotted in Fig. S5.

By applying this method, we successfully tracked 10 primary volatile species involved in the Cu-catalyzed CO₂RR using DEMS at a temporal resolution of ~400 ms; formate and acetate products were not detected, as they do not pervaporate. Fig. 3 shows the typical linear sweep voltammetry (LSV) curve recorded on a Cu/PTFE electrode in 0.1 M CO₂-saturated CsHCO₃ electrolyte at a scan rate of 5 mV s⁻¹, together with the relevant deconvoluted DEMS spectra for the primary products and CO₂ reactant. It is notable that these mass ion current signals are directly proportional to the depletion and/or generation rates of the corresponding species, therefore, a semi-quantitative analysis could be achieved by comparing their relative intensities and potential dependence. In the negative-going potential sweep, H₂ by-product evolved at the smallest overpotential, around -0.5 V, while CO as the first noticeable CO₂RR product evolved at about -0.6 V, accompanied by the consumption of CO₂. Muted CO growth was noted below -0.9 V, together with the augmentation of C₂₊ products and CH₄ in the large overpotential region, validating the vital *CO hydrogenation pathway for producing multi-carbon products and CH₄. CH₄ and C₂H₄ are two major hydrocarbon products from the CO₂RR. Herein, we noted a preferential selectivity toward C₂H₄ over CH₄ throughout the potential window of interest, which is in good harmony with previous H-cell electrolysis results on polycrystalline Cu electrodes deploying CsHCO₃ electrolyte rather than its K⁺ or Na⁺ counterparts [52].

CH₃CHO and C₂H₅OH were two major C₂₊ oxygenates produced below -0.8 V, with a relatively low mass ion current and a retarded onset potential of CH₃CHO being noted. Significantly, since differences in the ionization probability, fragmentation pattern, and relative volatility could considerably alter the proportions of the different analytes (in our case, CH₃CHO and C₂H₅OH) in their characteristic DEMS signals, we compared the characteristic mass signal intensity for CH₃CHO and C₂H₅OH at a given concentration of 200 mM prior to this real-time DEMS study of the Cu-catalyzed CO₂RR. As shown in Fig. S4, ~3 times higher intensity was observed for the characteristic $m/z = 31$ of ethanol compared to the $m/z = 43$ of acetaldehyde, whereas an approximately 20-fold higher mass signal for the ethanol fragment at a deconvoluted $m/z = 31$ was noted compared to the acetaldehyde fragment at a deconvoluted $m/z = 43$, confirming the relatively higher C₂H₅OH abundance generated during the negative potential sweep. Given the high oxygen exchange reactivity between acetaldehyde and water in alkaline conditions [53], in our case the local alkalinity (*vide infra*), in addition to the electrochemical

reduction pathway, may have promoted the chemical disproportionation of CH_3CHO into $\text{C}_2\text{H}_5\text{OH}$ at potentials below -0.8 V [44, 54], explaining its relatively low abundance. The three C_3 oxygenates shared a similar profile, with an onset potential around -1.0 V, in which $\text{C}_2\text{H}_5\text{CHO}$ showed the highest generation rate at the cathode surface compared to $\text{CH}_2=\text{CHCH}_2\text{OH}$ and $\text{C}_3\text{H}_7\text{OH}$ (Fig. S5).

Local alkalinity effect versus cation effect

In the literature, the Cs^+ cation has been reported to effectively promote C–C coupling performance, due to its electrostatic interaction with certain CO_2RR intermediates [25, 55] and its modification of the local electric field strength [56, 57]. Recent studies also suggest an enlarged promotion effect with increasing cation concentration [25, 58]. In line with these observations, one intuitive question is whether or not simply increasing the electrolyte concentration could further improve this cation (local electric field) effect. We therefore switched the catholyte from CO_2 -saturated 0.1 M CsHCO_3 to 0.5 and 1.0 M CsHCO_3 and tracked the DEMS signals during identical LSVs (Fig. 4). Despite the sharp increase in current density from -64.4 to -123.5 mA cm^{-2} at -1.4 V, a similar CO_2 depletion ratio of 46.6 – 53.1% was noted upon increased electrolyte concentration, along with an order of magnitude higher H_2 mass ion current. This observed Faradaic current increase should be ascribed to the undesired HER rather than to CO_2RR rate enhancement. Furthermore, the CH_4 production rate significantly increased with increasing electrolyte concentration, whereas the C_2H_4 remained minimally affected (Fig. S6), leading to a decreased selectivity ratio for $\text{C}_2\text{H}_4/\text{CH}_4$, as shown in Fig. 4c. Concurrently, the production rate of $\text{C}_2\text{H}_5\text{OH}$, the representative C_{2+} oxygenate, also decreased with increasing CsHCO_3 concentration.

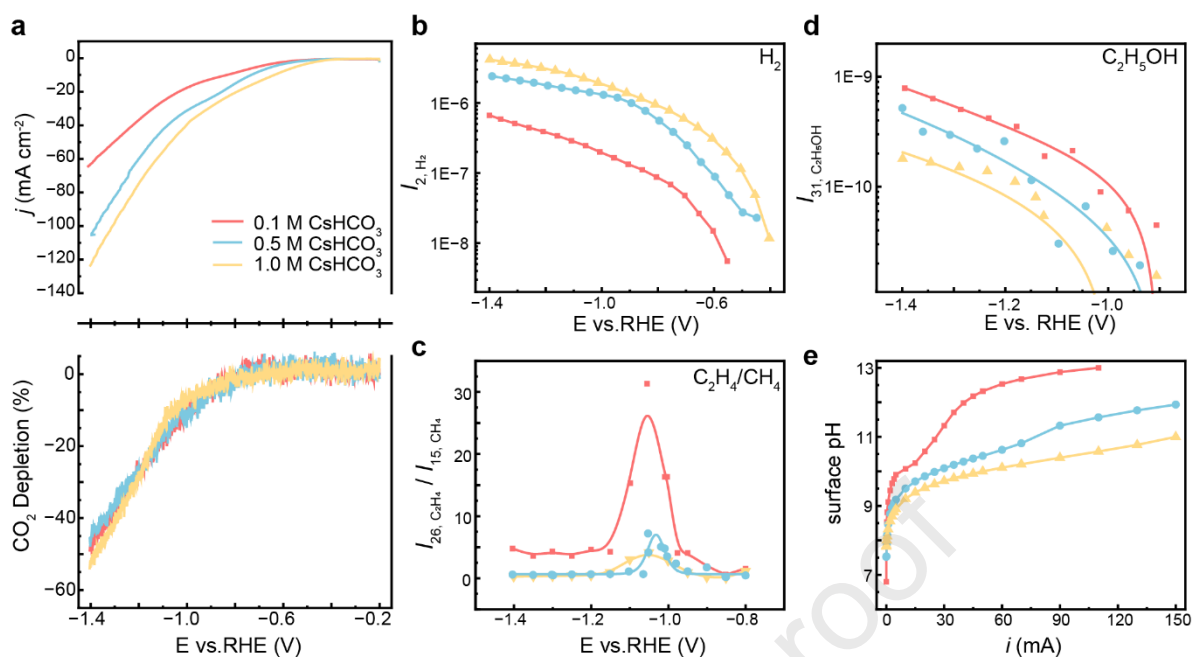


Fig. 4. The electrolyte concentration effect on the CO₂RR. (a) LSV and CO₂ depletion ratio plot recorded from -0.2 to -1.4 V vs. RHE at a scan rate of 5 mV s^{-1} in 0.1, 0.5, or 1.0 M CO₂-saturated CsHCO₃ at a constant flow rate of 128 mL min^{-1} , together with the mass ion current plots of (b) H₂, (c) C₂H₄ over CH₄, and (d) C₂H₅OH. (e) Simulated surface pH profile as a function of applied cathodic current at different electrolyte concentrations.

Drawing upon Hori's analysis [59], an increased local pH at a given cathodic potential should suppress CH₄ production but keep C₂ activity constant. To better interpret this local pH effect, we carried out a 1D simulation to tackle the surface pH variation as a function of applied cathodic current within 0.1, 0.5, or 1.0 M CsHCO₃ and with a given boundary layer thickness of $30 \text{ }\mu\text{m}$. As shown in Fig. 4e, the surface pH at -1.4 V was ca. 12.7, 11.6, and 11.0, respectively, correlating to a decreased C₂H₄/CH₄ ratio from 4.8 to 0.6 to 0.3. This pH dependence derived by our DEMS approach accords well with the steady-state electrolysis results [26, 60, 61]. Notably, under high CsHCO₃ concentration and large current density conditions, the bicarbonate anions directly served as proton donors to promote [H⁺]-mediated H₂ and CH₄ evolution reactions [62], even overriding the beneficial cation effect arising from the increased Cs⁺ concentration [25, 63]. The accelerated HER pathway, in turn, competed with the oxygenated pathway, suppressing ethanol production.

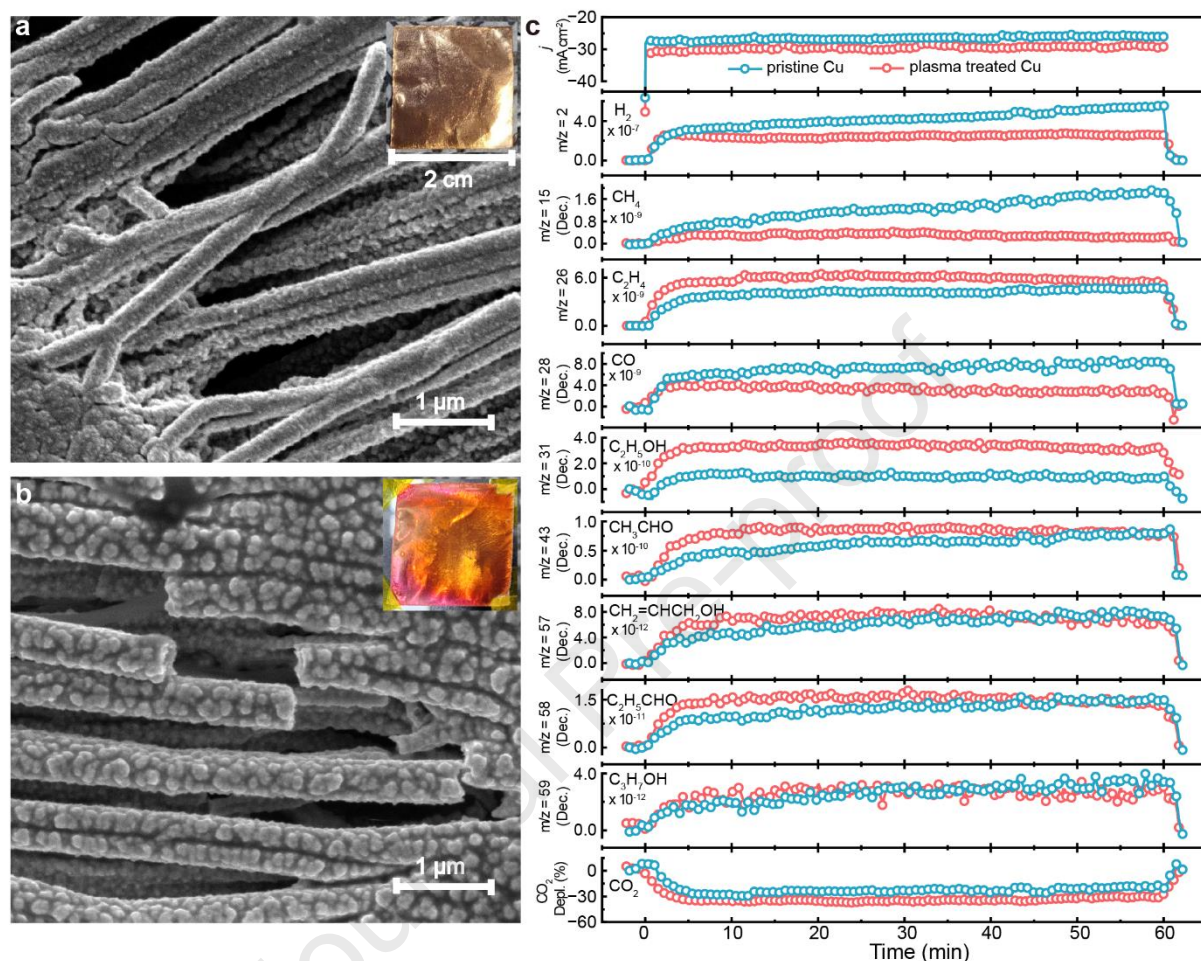
Cu surface topology effect

Fig. 5. Effect of O₂ plasma pre-treatment on the Cu-catalyzed CO₂RR. (a) SEM images for pristine and (b) Cu/PTFE electrodes treated with O₂ plasma for 150 s. (c) DEMS signal response during 1 h of potentiostatic electrolysis at -1.1 V in 0.1 M CO₂-saturated CsHCO₃ catholyte.

In addition to the above DEMS investigations of the polycrystalline Cu-catalyzed CO₂RR, we further treated a sputtered Cu/PTFE electrode with 150 s of O₂ plasma bombardment to generate undercoordinated surface sites [13, 64] and investigated how the surface topology affected the regulation of CO₂RR activity and selectivity. As depicted in Figs. 5a and 5b, the color of the Cu film electrode changed from light brown to reddish and showed a roughened, island-like structure at the microscopic level (Fig. S7). Prior to CO₂RR electrolysis, the O₂ plasma-treated Cu/PTFE was electrochemically reduced and stabilized at -0.6 V for 900 s (Fig.

S8), and the relevant electrochemical double layer capacitance (EDLC, Fig. S9) measurements suggest the surface area on the reduced Cu was double that of the pristine electrode. The electronic structural evolution of the surface Cu sites during plasma bombardment and electrochemical reduction was compared using core-level Cu 2p X-ray photoelectron spectra and LMM Auger spectra, which are presented in Fig. S10 [65].

Table 1. Relative ratio of averaged mass ion current for certain products on plasma-treated Cu over pristine Cu electrode.

Averaged $I_{\text{mass, product}}$	Relative ratio for mass signal change after bombardment
H ₂	-42%
CO	-54%
CH ₄	-76%
C ₂ H ₄	+43%
C ₂ H ₅ OH	+255%
CH ₃ CHO	+35%
CH ₂ =CHCH ₂ OH	+15%
C ₂ H ₅ CHO	+23%
C ₃ H ₇ OH	+2%
depleted CO ₂	+53%

Thereafter, we carried out a LSV scan from -0.2 to -1.4 V on the roughened electrode, similar to what had been done on pristine Cu, and compared their spectroelectrochemical responses. As shown in Fig. S11, a higher Faradaic current, accompanied by a higher CO₂ depletion ratio but a suppressed H₂ mass ion current, was observed on the roughened electrode, suggesting overall improved selectivity for the CO₂RR over the HER. Higher CO utilization was also noted, especially in the kinetic region between -0.7 and -1.1 V, leading to enhanced production rates for both C₂₊ hydrocarbons and oxygenates. More strikingly, the C₂H₄/CH₄ ratio, as representative of the C-C coupling performance, reached 173 at -1.0 V on the roughened Cu electrode and remained 4.0–10.8 times as high as on the pristine one (Fig. S12). Fig. 5c compares the potentiostatic electrolysis performance of these two Cu electrodes at -1.1 V; suppressed

formation of H₂, CH₄, and CO(g) on the plasma-treated Cu are notable during the 1 h of continuous electrolysis, whereas all other C₂₊ production rates were enhanced, especially for the ethanol species (Table 1). Compared to the previous probe-inlet online mass spectroscopic study on a Cu₂O-derived Cu electrode [66], we captured more comprehensive product distribution information at a higher signal-to-noise ratio, highlighting the high sensitivity of our current DEMS flow cell setup.

As already mentioned, the local pH should, intuitively, be a factor contributing to enhanced C₂₊/CH₄ selectivity through the *CO reduction pathway. At the given potential of -1.1 V, the average current rose from 30.0 mA (ca. 26.6 mA cm⁻²) on pristine Cu to 33.4 mA (ca. 29.6 mA cm⁻²) on bombarded Cu, giving rise to a surface pH increase from 11.66 to 11.79 (Fig. S13). Such a small change in the local pH is insufficient to explain the selectivity differences after oxygen plasma treatment [12, 14]. In contrast, our previous theoretical analysis and H-cell measurements revealed a higher fraction of undercoordinated Cu sites on the roughened surface, which preferentially bound CO, as well as a higher proportion of square Cu sites with neighboring steps that favored OC-COH adsorption toward C₂₊ production. In addition, the suppressed H₂ and CH₄ evolution on the roughened Cu electrode suggests a low surface coverage of *H but high local alkalinity, i.e., surface [HCO₃⁻] down to 3.4 mmol L⁻¹ but [CO₃²⁻] up to 79.4 mmol L⁻¹ at 33.4 mA, as shown in Fig. 6 and Fig. S14, in 0.1 M bicarbonate electrolyte, which was beneficial for the generation of C₂₊ oxygenates. In contrast, at the same current of 33.4 mA but in a 1.0 M bicarbonate electrolyte, a much higher surface [HCO₃⁻] of 761.9 mmol L⁻¹ was noted (Fig. S15), reinforcing our above analysis that the accelerated HER side reaction rate arose from the suppressed surface alkalinity (or the increased surface concentration of proton donors).

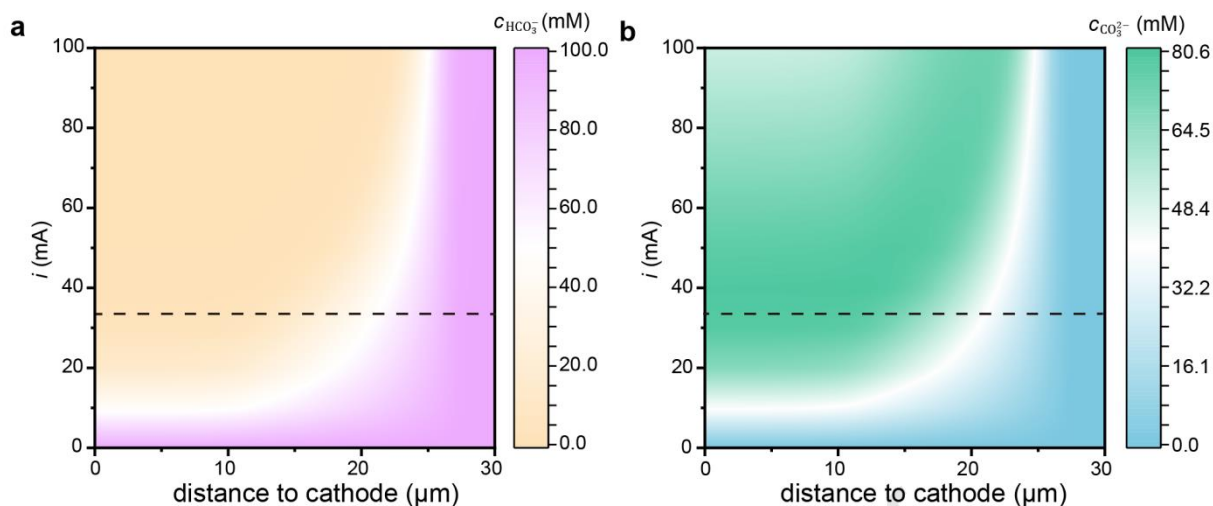


Fig. 6. Distribution profile of HCO_3^- and CO_3^{2-} as a function of distance to the cathode and applied current. A $30\ \mu\text{m}$, 1D diffusion model was used, given an initial boundary condition of $0.1\ \text{M}$ bulky bicarbonate electrolyte and $33\ \text{mM}$ aqueous CO_2 concentration.

Device performance validation

In view of the above local reaction environment effects from a fundamental spectroelectrochemical perspective, we further validated those tuning knobs on an anion exchange membrane electrode assembly (MEA) electrolyzer by considering three main advantages: (1) direct gaseous CO_2 fed at a facile mass transport rate, (2) high local alkalinity in the cathode vicinity without buffering the electrolyte, and (3) a roughened Cu surface with abundant undercoordinated sites. A humidified CO_2 flow was supplied on the cathodic side of a $1.5 \times 1.5\ \text{cm}^2$ O_2 -plasma treated Cu/PTFE electrode using an upstream mass flow controller, and the effluent was delivered through a downstream mass flow meter to the gas chromatograph for quantification. Specific attention was paid to the carbon balance in this high-rate CO_2RR scenario, as the generated OH^- at the cathode surface reacted with CO_2 , leading to a substantial reduction in the volumetric flow rate of effluent and overestimated FEs for gaseous products, as shown in Fig. S16 [67-69].

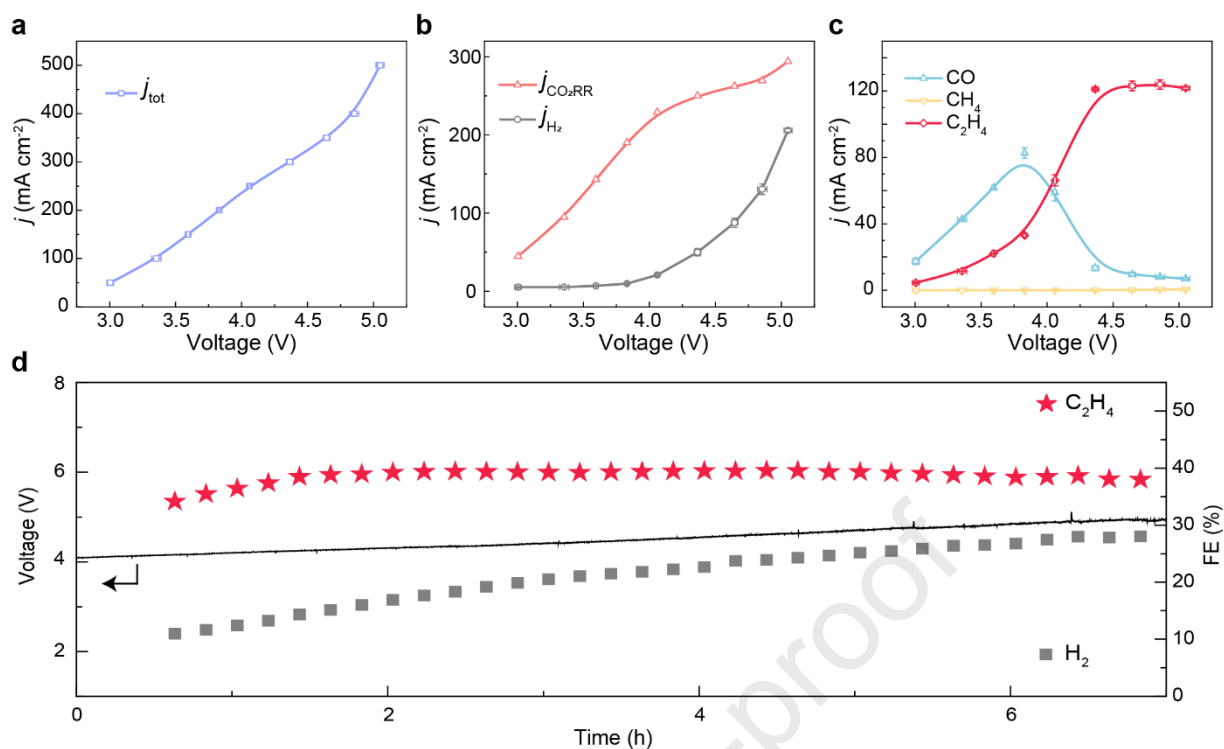


Fig. 7. Validating the local reaction environment effect on CO₂RR performance using an anion exchange MEA electrolyzer integrated with a $1.5 \times 1.5 \text{ cm}^2$ plasma-bombarded Cu/PTFE cathode. (a) Steady-state voltage profile during chronopotentiometric electrolysis, and the partial current densities for (b) the HER and CO₂RR, and (c) CO, CH₄, and C₂H₄. (e) Long-term electrolysis at a constant current density of 300 mA cm^{-2} .

Chronopotentiometric electrolysis was then carried out stepwise from 50 to 500 mA cm^{-2} with a full cell voltage ranging from 3.0 to 5.1 V (Fig. 7a), and the distribution of relevant gaseous products was plotted (Fig. S16) after rigorous flow-rate assessment. In the moderate voltage window below 4 V, H₂ FEs were suppressed below 10%, indicating an overwhelming CO₂RR selectivity via modulation of the local reaction environment. CO was the major CO₂RR product, with an FE of up to 42% at 100 mA cm^{-2} ; it was readily converted into C₂H₄ under higher applied current densities, where CH₄ FEs remained below 0.1% throughout the operating window. A maximum C₂H₄ FE of up to 40.4% was achieved at $\sim 4.35 \text{ V}$, with a partial current density of 115 mA cm^{-2} , showing a plateau around 120 mA cm^{-2} from 4.3 to 5.1 V as well as a wide voltage window above 0.9 V for selective C₂H₄ production (FE > 30%). It is noteworthy that compared to conventional aqueous electrolysis, the present MEA electrolyzer configuration using a Cu/PTFE gas diffusion electrode largely mitigated, but did not eliminate, the CO₂ mass transport limitation, with an order of magnitude enhanced CO₂ reduction rate. The CO₂RR

stability for this MEA integrated with a bombarded Cu/PTFE electrode was then evaluated at 300 mA cm^{-2} (Figs. 7d and S17), demonstrating a stable C_2H_4 selectivity of around 38% throughout 7 h of continuous electrolysis. Nevertheless, the cell voltage gradually increased to $\sim 4.9 \text{ V}$, and the FE for H_2 rose from 11% to 28%, potentially due to the surface reconstruction of the Cu electrode, the membrane's decreased ionic conductivity upon HCO_3^- exchange, and/or salt precipitation. Studying in depth the degraded energy efficiency and overall CO_2RR selectivity is a possibility for future work, with the potential to formulate a comprehensive triple-phase boundary model for high-rate CO_2RR conditions.

Conclusions

An investigation combining online differential electrochemical mass spectroscopy, computational fluid dynamics, and numerical simulations has been applied to analyze the local reaction environment effect for steering CO_2 electrolysis selectivity over Cu electrodes. The direct membrane-inlet configuration and relevant deconvolution protocols enabled the successful tracking of 10 primary volatile species during the CO_2RR at a temporal resolution of $\sim 400 \text{ ms}$. Our DEMS results suggest that boosting CO_2 mass transport and local alkalinity, as well as increasing the electrode's surface roughness by plasma bombardment, can effectively aid in suppressing the H_2 evolution side reaction and the $^*\text{CO}$ -to- CH_4 pathway, thus facilitating the generation of C_{2+} products. These hints from fundamental spectroelectrochemistry were also validated using a bombarded Cu/PTFE gas diffusion electrode integrated into an anion exchange membrane electrolyzer, demonstrating a C_2H_4 Faradaic efficiency of up to 40.4% and a partial current density of 121 mA cm^{-2} . This work highlights the vital role of the local reaction environment in defining CO_2RR activity and selectivity, shedding light on real-world CO_2 valorization infrastructure.

Methods

Electrode preparation

Working electrodes of ca. 300 nm Cu film sputtered on either PTFE membrane (20 nm pore

size, Cobetter) substrates were prepared using a Denton sputter system, at a deposition rate of 1 Å/s to an effective thickness of 300 nm under a 0.5 Pa Ar atmosphere (99.999%, Air Liquide). Prior to the magnetron sputtering, hydrophobic PTFE membrane was pre-treated with acetone, methanol, and Milli-Q water (18.2 MΩ·cm) in succession and dried in a stream of flowing N₂ (99.999%, Keju Chemistry). For O₂ plasma pre-treatment, the Cu/PTFE electrodes were placed in an HM-Plasma2L (Hongming Instrument) evacuated with a mechanical pump to ~10 Torr, then exposed to a 150 W plasma for 150 s under an 80 sccm O₂ flow (99.999%, Air Liquide).

Material characterizations

The surface morphology images were filmed with a NOVA NanoSEM 230 field-emission scanning electron microscope, using an electron beam energy of 5 kV and a spot size of 3.0 nm with a magnification ranging from 5 to 20 k. The near-surface composition of the Cu electrodes was probed by X-ray photoelectron spectroscopy (XPS) with a Kratos AXIS Ultra DLD spectrometer, using monochromatic Al K α radiation (1486.6 eV) and a low energy flood gun as the neutralizer. The Casa XPS program was employed for surface component content analysis, with the binding energies calibrated with reference to the C 1s peak at 284.8 eV.

Online DEMS measurements

Online DEMS measurements were run on a Hiden HPR-40 quadrupole mass spectrometer equipped with a secondary electron multiplier detector. A cage voltage of 3 V, an electron energy of 70 eV, and an emission current of 500 μ A were set at the ionization source, together with a detector voltage of 1200 V for recording real-time mass spectra. Prior to data acquisition, DEMS background signals were pre-stabilized for 1 h and subtracted from m/z signals for quantitative analysis. The setup of the DEMS flow cell is illustrated in Fig. S1; it consisted of a 1.13 cm⁻² Cu/PTFE working electrode, a Pt gauze counter electrode, and a leak-free Ag/AgCl reference electrode (Innovative).

Prior to each experiment, the flow cell was sonicated in 20 wt% nitric acid (diluted from 70% concentrated HNO₃, AR, Sinopharm Chemical Reagent) and boiled in Milli-Q water for cleaning. A certain amount of Cs₂CO₃ (99.99%, Adamas-Beta) was dissolved in Milli-Q water to achieve a concentration of 0.05 M, then the mixture was further purified by electrolysis

between two graphite rods at 0.1 mA for 24 h to remove trace amount of metal ion impurities. Next, 50 sccm CO₂ (99.995%, Air Liquide) was bubbled for at least 30 min to obtain a 0.1 M CO₂-saturated CsHCO₃ electrolyte. Electrochemical responses were recorded on a Biologic VSP-300 potentiostat. The solution resistance (R_u) was determined by potentiostatic electrochemical impedance spectroscopy at frequencies ranging from 0.1 Hz to 200 kHz and was compensated *in situ* at the 85% level by a potentiostat during linear potential sweeps. Unless otherwise indicated, all potentials in this work were converted to the RHE scale as E (vs. RHE) = E (vs Ag/AgCl) + 0.197 V + 0.0591 × pH_{bulk}.

Computational methods

The three-dimensional computational fluid dynamics simulations and the transport of species in the cathodic boundary layer were solved using COMSOL Multiphysics 5.6. A synopsis of the modeling details is given in Supplementary Notes 1 and 2.

MEA measurements

For the practical membrane electrode assembly electrolyzer tests, a 1.5 × 1.5 cm² Cu/PTFE electrode treated with O₂ plasma for 150 s was used as the CO₂RR cathode, and an IrO₂-coated Ti felt was used as the anode. A quaternary ammonia poly (N-methyl-piperidine-*co-p*-terphenyl) anion exchange membrane (QAPPT, EVE Energy) was sandwiched between the two gas diffusion electrodes to separate the chambers. The QAPPT membrane was pre-activated in 1 M KOH (AR, Sinopharm Chemical Reagent) at 60 °C for 24 h prior to usage. 50 sccm humidified CO₂ was delivered through the cathodic Ti flow field, while the anolyte CsOH (99.9% Meryer) was circulated at a flow rate of 1.8 mL min⁻¹.

The effluent from the cathodic chamber was analyzed with a Shimadzu 2014 gas chromatograph equipped with a thermal conductivity detector (TCD) for H₂ concentration quantification and a flame ionization detector (FID) coupled with a methanizer for quantifying the CO and hydrocarbon concentrations. The signal response of the TCD and FID were calibrated by analyzing a series of standard gas mixtures, as shown in Fig. S18. The FE of a given reduction product was calculated as follows:

$$FE_i = \frac{x_i v n F}{V \times j} \times 100\%$$

where x_i is the volume fraction of species i as determined by online GC, v is the flow rate calibrated by a mass flow meter (Alicat), n is the electron transfer number, F is the Faradaic constant, V is the molar volume of an ideal gas under CO₂RR operating conditions, and j is the total current density. The liquid products were collected by placing a gas-tight cold trap (cooled in an ice-water bath at 0 °C) in between the cathodic effluent outlet and the GC inlet, then quantified with a 1D ¹H NMR spectrum using a Bruker Avance NEO 400 MHz spectrometer. In brief, 60 μL of collected electrolyte was diluted to 600 μL using Milli-Q water and mixed with 100 μL of D₂O (Sigma Aldrich, 99.9 at.% deuterium) and 0.05 μL dimethylsulfoxide (as an internal standard, Sigma Aldrich, 99.9%).

Author contributions

K.J. conceptualized and supervised the project. K.Y. and K.J. developed and performed electrodes preparation, conducted the (spectro)electrochemical measurements and the related data processing. K.Y. performed materials characterization with the help of G.Z., B.N. C.D. and X.Z. Computational simulations and relevant analysis were carried out by K.Y., L.G. and C.Z. K.Y., W.B.C. and K.J. wrote the paper. All authors discussed the results and commented on the paper.

Conflicts of Interest

The authors declare no conflict of interest.

Acknowledgements

This work was supported by the National Key R&D Program of China (2022YFB4102000, 2022YFA1505100, 2022YFA1503803), the NSFC (22002088), the Shanghai Sailing Program (20YF1420500), and the Shanghai Science and Technology Innovation Action Plan (22dz1205500).

References

[1] O.S. Bushuyev, P. De Luna, C.T. Dinh, L. Tao, G. Saur, J. van de Lagemaat, S.O. Kelley, E.H. Sargent, What

should we make with CO₂ and how can we make it?, *Joule* 2 (2018) 825-832.

- [2] Z.W. Seh, J. Kibsgaard, C.F. Dickens, I. Chorkendorff, J.K. Norskov, T.F. Jaramillo, Combining theory and experiment in electrocatalysis: Insights into materials design, *Science* 355 (2017) 6321.
- [3] C. Hepburn, E. Adlen, J. Beddington, E.A. Carter, S. Fuss, N. Mac Dowell, J.C. Minx, P. Smith, C.K. Williams, The technological and economic prospects for CO₂ utilization and removal, *Nature* 575 (2019) 87-97.
- [4] S. Nitopi, E. Bertheussen, S.B. Scott, X. Liu, A.K. Engstfeld, S. Horch, B. Seger, I.E.L. Stephens, K. Chan, C. Hahn, J.K. Norskov, T.F. Jaramillo, I. Chorkendorff, Progress and perspectives of electrochemical CO₂ reduction on copper in aqueous electrolyte, *Chem. Rev.* 119 (2019) 7610-7672.
- [5] I.E.L. Stephens, K. Chan, A. Bagger, S.W. Boettcher, J. Bonin, E. Boutin, A.K. Buckley, R. Buonsanti, E.R. Cave, X. Chang, S.W. Chee, A.H.M. da Silva, P. de Luna, O. Einsle, B. Endródi, M. Escudero-Escribano, J.V. Ferreira de Araujo, M.C. Figueiredo, C. Hahn, K.U. Hansen, S. Haussener, S. Hunegnaw, Z. Huo, Y.J. Hwang, C. Janáky, B.S. Jayathilake, F. Jiao, Z.P. Jovanov, P. Karimi, M.T.M. Koper, K.P. Kuhl, W.H. Lee, Z. Liang, X. Liu, S. Ma, M. Ma, H.-S. Oh, M. Robert, B.R. Cuenya, J. Rossmeisl, C. Roy, M.P. Ryan, E.H. Sargent, P. Sebastián-Pascual, B. Seger, L. Steier, P. Strasser, A.S. Varela, R.E. Vos, X. Wang, B. Xu, H. Yadegari, Y. Zhou, 2022 roadmap on low temperature electrochemical CO₂ reduction, *J. Phys. Energy* 4 (2022) 042003.
- [6] A. Bagger, W. Ju, A.S. Varela, P. Strasser, J. Rossmeisl, Electrochemical CO₂ reduction: a classification problem, *ChemPhysChem* 18 (2017) 3266-3273.
- [7] M. Dunwell, W. Luc, Y. Yan, F. Jiao, B. Xu, Understanding surface-mediated electrochemical reactions: CO₂ reduction and beyond, *ACS Catal.* 8 (2018) 8121-8129.
- [8] R.G. Grim, Z. Huang, M.T. Guarnieri, J.R. Ferrell, L. Tao, J.A. Schaidle, Transforming the carbon economy: challenges and opportunities in the convergence of low-cost electricity and reductive CO₂ utilization, *Energy Environ. Sci.* 13 (2020) 472-494.
- [9] N. Hoshi, M. Kato, Y. Hori, Electrochemical reduction of CO₂ on single crystal electrodes of silver Ag (111), Ag (100) and Ag (110), *J. Electroanal. Chem.* 440 (1997) 283-286.
- [10] C. Hahn, T. Hatsukade, Y.G. Kim, A. Vailionis, J.H. Baricuatro, D.C. Higgins, S.A. Nitopi, M.P. Soriaga, T.F. Jaramillo, Engineering Cu surfaces for the electrocatalytic conversion of CO₂: Controlling selectivity toward oxygenates and hydrocarbons, *Proc. Natl. Acad. Sci. U.S.A.* 114 (2017) 5918-5923.
- [11] G. Zhang, Z.J. Zhao, D. Cheng, H. Li, J. Yu, Q. Wang, H. Gao, J. Guo, H. Wang, G.A. Ozin, T. Wang, J. Gong, Efficient CO₂ electroreduction on facet-selective copper films with high conversion rate, *Nat. Commun.* 12 (2021) 5745.
- [12] K. Jiang, R.B. Sandberg, A.J. Akey, X. Liu, D.C. Bell, J.K. Nørskov, K. Chan, H. Wang, Metal ion cycling of Cu foil for selective C–C coupling in electrochemical CO₂ reduction, *Nat. Catal.* 1 (2018) 111-119.
- [13] K. Jiang, Y. Huang, G. Zeng, F.M. Toma, W.A. Goddard, A.T. Bell, Effects of surface roughness on the electrochemical reduction of CO₂ over Cu, *ACS Energy Lett.* 5 (2020) 1206-1214.
- [14] J.A. Gauthier, J.H. Stenlid, F. Abild-Pedersen, M. Head-Gordon, A.T. Bell, The Role of roughening to enhance selectivity to C₂₊ products during CO₂ electroreduction on Copper, *ACS Energy Lett.* 6 (2021) 3252-3260.
- [15] H.S. Zhengxiang Gu, Zheng Chen, Yaoyue Yang, Chao Yang, Yali Ji, Yuhang Wang, J.L. Chan Zhu, Jun Li, Tsun-Kong Sham, Xin Xu, and Gengfeng Zheng, Efficient electrocatalytic CO₂ reduction to C₂₊ alcohols at defect-site-rich Cu surface, *Joule* 5 (2021) 429-440.
- [16] C. Chen, S. Yu, Y. Yang, S. Louisia, I. Roh, J. Jin, S. Chen, P.-C. Chen, Y. Shan, P. Yang, Exploration of the bio-analogous asymmetric C–C coupling mechanism in tandem CO₂ electroreduction, *Nat. Catal.* 5 (2022) 878-887.
- [17] Y. Xie, P. Ou, X. Wang, Z. Xu, Y.C. Li, Z. Wang, J.E. Huang, J. Wicks, C. McCallum, N. Wang, Y. Wang, T. Chen, B.T.W. Lo, D. Sinton, J.C. Yu, Y. Wang, E.H. Sargent, High carbon utilization in CO₂ reduction to multi-carbon products in acidic media, *Nat. Catal.* 5 (2022) 564-570.
- [18] P. Wang, H. Yang, C. Tang, Y. Wu, Y. Zheng, T. Cheng, K. Davey, X. Huang, S.Z. Qiao, Boosting

electrocatalytic CO₂-to-ethanol production via asymmetric C-C coupling, *Nat. Commun.* 13 (2022) 3754.

[19] Y. Ji, Z. Chen, R. Wei, C. Yang, Y. Wang, J. Xu, H. Zhang, A. Guan, J. Chen, T.-K. Sham, J. Luo, Y. Yang, X. Xu, G. Zheng, Selective CO-to-acetate electroreduction via intermediate adsorption tuning on ordered Cu–Pd sites, *Nat. Catal.* 5 (2022) 251-258.

[20] D.L. Meng, M.D. Zhang, D.H. Si, M.J. Mao, Y. Hou, Y.B. Huang, R. Cao, Highly selective tandem electroreduction of CO₂ to ethylene over atomically isolated nickel-nitrogen site/copper nanoparticle catalysts, *Angew. Chem. Int. Ed.* 60 (2021) 25485-25492.

[21] C. Kim, J.C. Bui, X. Luo, J.K. Cooper, A. Kusoglu, A.Z. Weber, A.T. Bell, Tailored catalyst microenvironments for CO₂ electroreduction to multicarbon products on copper using bilayer ionomer coatings, *Nat. Energy* 6 (2021) 1026-1034.

[22] F. Li, A. Thevenon, A. Rosas-Hernandez, Z. Wang, Y. Li, C.M. Gabardo, A. Ozden, C.T. Dinh, J. Li, Y. Wang, J.P. Edwards, Y. Xu, C. McCallum, L. Tao, Z.Q. Liang, M. Luo, X. Wang, H. Li, C.P. O'Brien, C.S. Tan, D.H. Nam, R. Quintero-Bermudez, T.T. Zhuang, Y.C. Li, Z. Han, R.D. Britt, D. Sinton, T. Agapie, J.C. Peters, E.H. Sargent, Molecular tuning of CO₂-to-ethylene conversion, *Nature* 577 (2020) 509-513.

[23] K. Xu, J. Li, F. Liu, W. Xu, T. Zhao, F. Cheng, Steering CO₂ electroreduction selectivity towards CH₄ and C₂H₄ on a tannic acid-modified Cu electrode, *Mater. Chem. Front.* 7 (2023) 1395-1402.

[24] M.C.O. Monteiro, F. Dattila, N. Lopez, M.T.M. Koper, The role of cation acidity on the competition between hydrogen evolution and CO₂ reduction on gold electrodes, *J. Am. Chem. Soc.* 144 (2022) 1589-1602.

[25] M.C.O. Monteiro, F. Dattila, B. Hagedoorn, R. García-Muelas, N. López, M.T.M. Koper, Absence of CO₂ electroreduction on copper, gold and silver electrodes without metal cations in solution, *Nat. Catal.* 4 (2021) 654–662.

[26] J. Resasco, Y. Lum, E. Clark, J.Z. Zeledon, A.T. Bell, Effects of Anion identity and concentration on electrochemical reduction of CO₂, *ChemElectroChem* 5 (2018) 1064-1072.

[27] C.M. Gunathunge, V.J. Ovalle, M.M. Waegle, Probing promoting effects of alkali cations on the reduction of CO at the aqueous electrolyte/copper interface, *Phys. Chem. Chem. Phys.* 19 (2017) 30166-30172.

[28] J. Li, G. Chen, Y. Zhu, Z. Liang, A. Pei, C.-L. Wu, H. Wang, H.R. Lee, K. Liu, S. Chu, Y. Cui, Efficient electrocatalytic CO₂ reduction on a three-phase interface, *Nat. Catal.* 1 (2018) 592-600.

[29] C. Zhu, Y. Song, X. Dong, G. Li, A. Chen, W. Chen, G. Wu, S. Li, W. Wei, Y. Sun, Ampere-level CO₂ reduction to multicarbon products over a copper gas penetration electrode, *Energy Environ. Sci.* 15 (2022) 5391-5404.

[30] P. Wei, D. Gao, T. Liu, H. Li, J. Sang, C. Wang, R. Cai, G. Wang, X. Bao, Coverage-driven selectivity switch from ethylene to acetate in high-rate CO₂/CO electrolysis, *Nat. Nanotechnol.* 18 (2023) 299-306.

[31] Y. Huang, A.D. Handoko, P. Hirunsit, B.S. Yeo, Electrochemical reduction of CO₂ using copper single-crystal surfaces: effects of CO* coverage on the selective formation of ethylene, *ACS Catal.* 7 (2017) 1749-1756.

[32] C. Hahn, T.F. Jaramillo, Using microenvironments to control reactivity in CO₂ electrocatalysis, *Joule* 4 (2020) 292-294.

[33] J. Chen, L. Wang, Effects of the catalyst dynamic changes and influence of the reaction environment on the performance of electrochemical CO₂ reduction, *Adv. Mater.* (2021) e2103900.

[34] X. Zhou, H. Liu, B.Y. Xia, K. Ostrikov, Y. Zheng, S.Z. Qiao, Customizing the microenvironment of CO₂ electrocatalysis via three-phase interface engineering, *SmartMat* 3 (2022) 111-129.

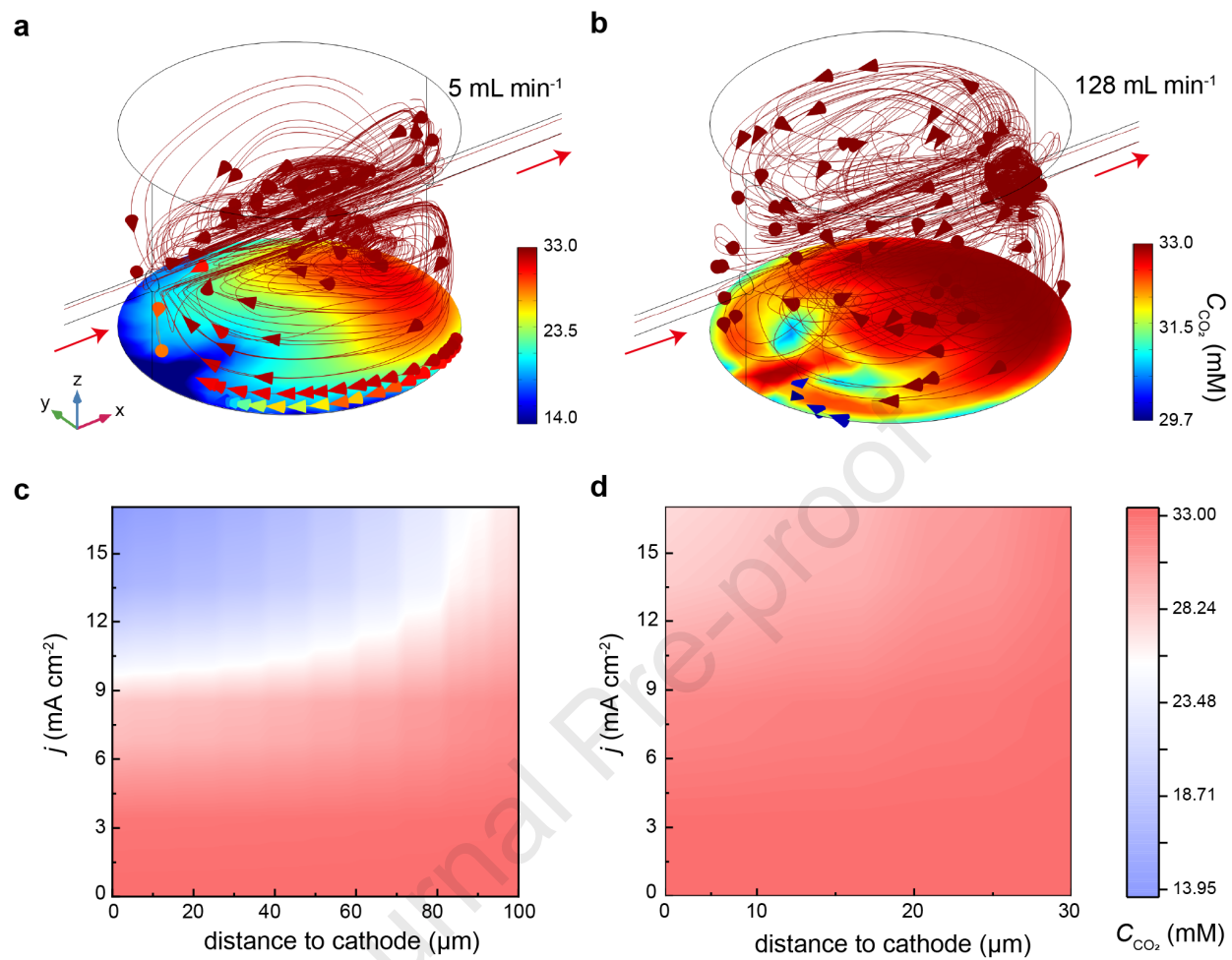
[35] H. Li, K. Jiang, S.-Z. Zou, W.-B. Cai, Fundamental aspects in CO₂ electroreduction reaction and solutions from in situ vibrational spectroscopies, *Chin. J. Catal.* 43 (2022) 2772-2791.

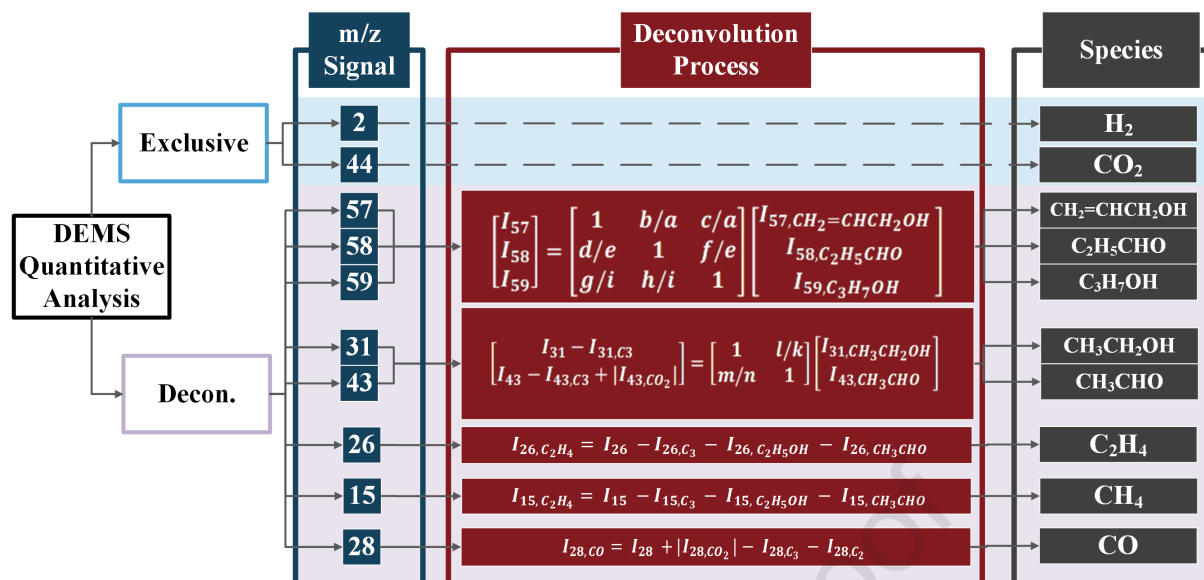
[36] H.-S. Su, X. Chang, B. Xu, Surface-enhanced vibrational spectroscopies in electrocatalysis: Fundamentals, challenges, and perspectives, *Chin. J. Catal.* 43 (2022) 2757-2771.

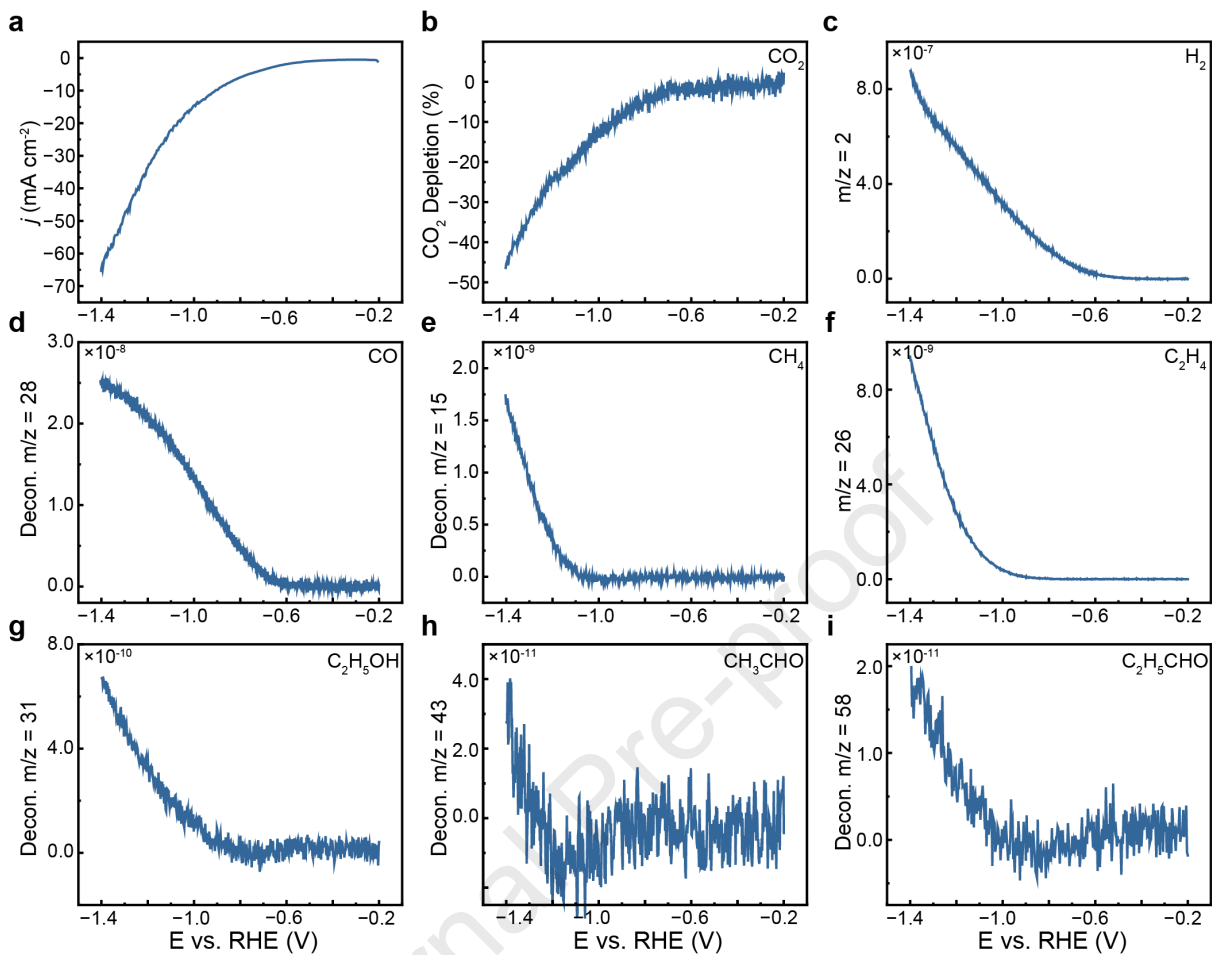
[37] M. Farmand, A.T. Landers, J.C. Lin, J.T. Feaster, J.W. Beeman, Y. Ye, E.L. Clark, D. Higgins, J. Yano, R.C. Davis, A. Mehta, T.F. Jaramillo, C. Hahn, W.S. Drisdell, Electrochemical flow cell enabling operando probing of

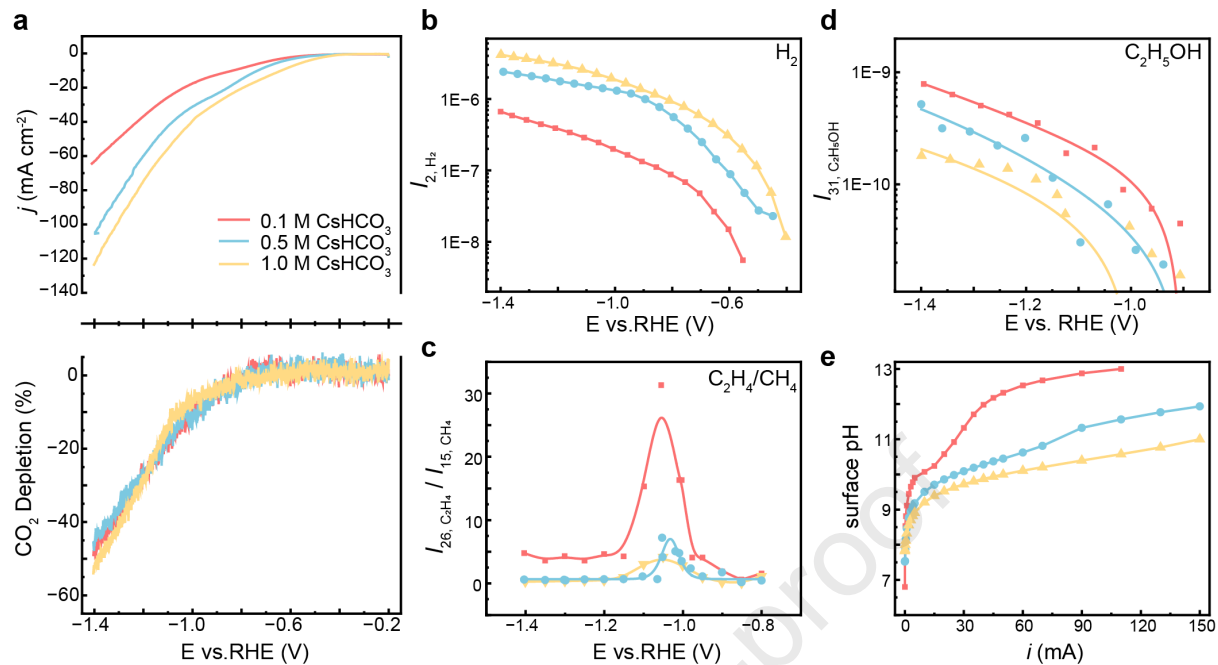
- electrocatalyst surfaces by X-ray spectroscopy and diffraction, *Phys. Chem. Chem. Phys.* 21 (2019) 5402-5408.
- [38] B.B. Sarma, F. Maurer, D.E. Doronkin, J.D. Grunwaldt, Design of single-stom catalysts and tracking their fate using operando and advanced X-ray spectroscopic tools, *Chem. Rev.* 123 (2023) 379-444.
- [39] Y. Zhao, X.-G. Zhang, N. Bodappa, W.-M. Yang, Q. Liang, P.M. Radjenovica, Y.-H. Wang, Y.-J. Zhang, J.-C. Dong, Z.-Q. Tian, J.-F. Li, Elucidating electrochemical CO₂ reduction reaction processes on Cu(hkl) single-crystal surfaces by in situ Raman spectroscopy, *Energy Environ. Sci.* 15 (2022) 3968-3977.
- [40] X. Li, S. Wang, L. Li, Y. Sun, Y. Xie, Progress and perspective for in situ studies of CO₂ reduction, *J. Am. Chem. Soc.* 142 (2020) 9567-9581.
- [41] P.Z. ZHAO Zhiwei, Differential electrochemical mass spectroscopy: A pivotal technology for investigating lithium-ion batteries, *Energy Storage Sci. Technol.* 8 (2019) 1-13.
- [42] Y.-H. Hong, Z.-Y. Zhou, M. Zhan, Y.-C. Wang, Y. Chen, S.-C. Lin, M. Rauf, S.-G. Sun, Liquid-inlet online electrochemical mass spectrometry for the in operando monitoring of direct ethanol fuel cells, *Electrochem. Commun.* 87 (2018) 91-95.
- [43] Q. Tao, Y.-L. Zheng, D.-C. Jiang, Y.-X. Chen, Z. Jusys, R.J. Behm, Interaction of C₁ Molecules with a Pt electrode at open circuit potential: a combined infrared and mass spectroscopic study, *J. Phys. Chem. C* 118 (2014) 6799-6808.
- [44] K.J.P. Schouten, Y. Kwon, C.J.M. van der Ham, Z. Qin, M.T.M. Koper, A new mechanism for the selectivity to C₁ and C₂ species in the electrochemical reduction of carbon dioxide on copper electrodes, *Chem. Sci.* 2 (2011) 1902-1909.
- [45] E.L. Clark, A.T. Bell, Direct observation of the local reaction environment during the electrochemical reduction of CO₂, *J. Am. Chem. Soc.* 140 (2018) 7012-7020.
- [46] B. Hasa, M. Jouny, B.H. Ko, B. Xu, F. Jiao, Flow electrolyzer mass spectrometry with a gas-diffusion electrode design, *Angew. Chem. Int. Ed.* 60 (2020). 3277-3282
- [47] M. Löffler, P. Khanipour, N. Kulyk, K.J.J. Mayrhofer, I. Katsounaros, Insights into liquid product formation during carbon dioxide reduction on copper and oxide-derived copper from quantitative real-time measurements, *ACS Catal.* 10 (2020) 6735-6740.
- [48] K. Ye, G. Zhang, X.-Y. Ma, C. Deng, X. Huang, C. Yuan, G. Meng, W.-B. Cai, K. Jiang, Resolving local reaction environment toward an optimized CO₂-to-CO conversion performance, *Energy Environ. Sci.* 15 (2022) 749-759.
- [49] K.P. Kuhl, E.R. Cave, D.N. Abram, T.F. Jaramillo, New insights into the electrochemical reduction of carbon dioxide on metallic copper surfaces, *Energy Environ. Sci.* 5 (2012) 7050-7059.
- [50] G. Wen, B. Ren, X. Wang, D. Luo, H. Dou, Y. Zheng, R. Gao, J. Gostick, A. Yu, Z. Chen, Continuous CO₂ electrolysis using a CO₂ exsolution-induced flow cell, *Nat. Energy*, 7 (2022) 978-988.
- [51] <https://webbook.nist.gov/chemistry/>.
- [52] J. Resasco, L.D. Chen, E. Clark, C. Tsai, C. Hahn, T.F. Jaramillo, K. Chan, A.T. Bell, Promoter Effects of alkali metal cations on the electrochemical reduction of carbon dioxide, *J. Am. Chem. Soc.* 139 (2017) 11277-11287.
- [53] B. Hasa, M. Jouny, B.H. Ko, B. Xu, F. Jiao, Flow Electrolyzer Mass spectrometry with a gas-diffusion electrode design, *Angew. Chem. Int. Ed.* 60 (2021) 3277-3282.
- [54] Y.Y. Birdja, M.T.M. Koper, The importance of cannizzaro-type reactions during electrocatalytic reduction of carbon dioxide, *J. Am. Chem. Soc.* 139 (2017) 2030-2034.
- [55] V.J. Ovalle, Y.-S. Hsu, N. Agrawal, M.J. Janik, M.M. Waegle, Correlating hydration free energy and specific adsorption of alkali metal cations during CO₂ electroreduction on Au, *Nat. Catal.* 5 (2022) 624-632.
- [56] A. Xu, N. Govindarajan, G. Kastlunger, S. Vijay, K. Chan, Theories for electrolyte effects in CO₂ electroreduction, *Acc. Chem. Res.* 55 (2022) 495-503.
- [57] J.C. Bui, C. Kim, A.J. King, O. Romiluyi, A. Kusoglu, A.Z. Weber, A.T. Bell, Engineering catalyst-electrolyte

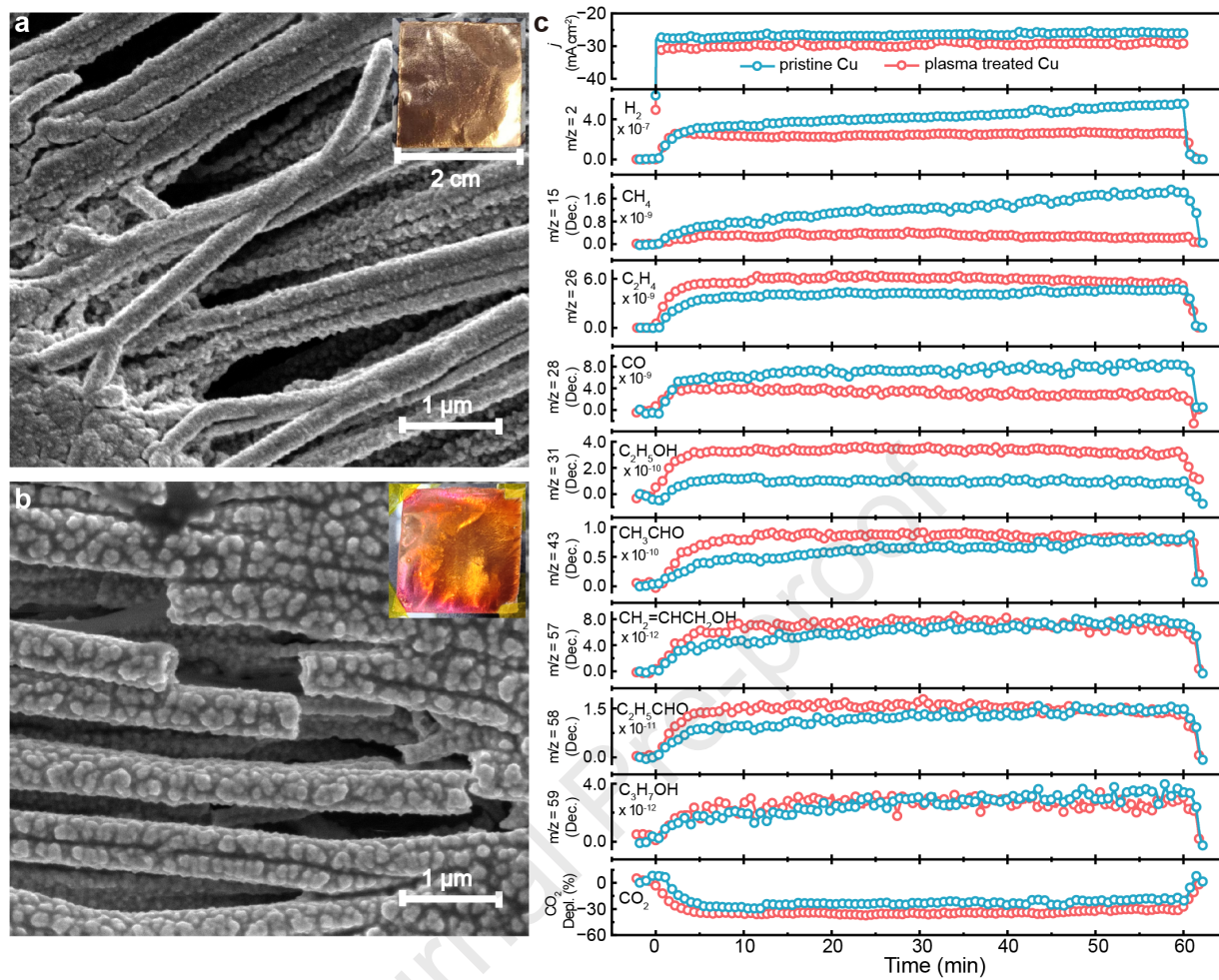
- microenvironments to optimize the activity and selectivity for the electrochemical reduction of CO₂ on Cu and Ag, *Acc. Chem. Res.* 55 (2022) 484-494.
- [58] J. Li, D. Wu, A.S. Malkani, X. Chang, M.J. Cheng, B. Xu, Q. Lu, Hydroxide is not a promoter of C₂₊ product formation in the electrochemical reduction of CO on copper, *Angew. Chem. Int. Ed.* 59 (2020) 4464-4469.
- [59] Y. Hori, R. Takahashi, Y. Yoshinami, A. Murata, Electrochemical reduction of CO at a copper electrode, *J. Phys. Chem. B* 101 (1997) 7075-7081.
- [60] Y. Hori, A. Murata, R. Takahashi, Formation of hydrocarbons in the electrochemical reduction of carbon dioxide at a copper electrode in aqueous solution, *J. Chem. Soc. Faraday Trans.* 85 (1989) 2309-2326.
- [61] K. Yang, R. Kas, W. A. Smith, In situ infrared spectroscopy reveals persistent alkalinity near electrode surfaces during CO₂ electroreduction, *J. Am. Chem. Soc.* 141 (2019) 15891-15900.
- [62] G. Marcandalli, M.C.O. Monteiro, A. Goyal, M.T.M. Koper, Electrolyte effects on CO₂ electrochemical reduction to CO, *Acc. Chem. Res.* 55 (2022) 1900-1911.
- [63] J. Li, D. Wu, A.S. Malkani, X. Chang, M.J. Cheng, B. Xu, Q. Lu, Hydroxide Is not a promoter of C₂₊ product formation in the electrochemical reduction of CO on copper, *Angew. Chem. Int. Ed.* 59 (2020) 4464-4469.
- [64] H. Mistry, A.S. Varela, C.S. Bonifacio, I. Zegkinoglou, I. Sinev, Y.W. Choi, K. Kisslinger, E.A. Stach, J.C. Yang, P. Strasser, B.R. Cuenya, Highly selective plasma-activated copper catalysts for carbon dioxide reduction to ethylene, *Nat. Commun.* 7 (2016) 12123.
- [65] H. Li, T. Liu, P. Wei, L. Lin, D. Gao, G. Wang, X. Bao, High-rate CO₂ electroreduction to C₂₊ products over a copper-copper iodide catalyst, *Angew. Chem. Int. Ed.* 60 (2021) 14329-14333.
- [66] R. Kas, R. Kortlever, A. Milbrat, M.T.M. Koper, G. Mul, J. Baltrusaitis, Electrochemical CO₂ reduction on Cu₂O-derived copper nanoparticles: controlling the catalytic selectivity of hydrocarbons, *Phys. Chem. Chem. Phys.* 16 (2014) 12194-12201.
- [67] Z.-Z. Niu, L.-P. Chi, R. Liu, Z. Chen, M.-R. Gao, Rigorous assessment of CO₂ electroreduction products in a flow cell, *Energy Environ. Sci.* 14 (2021) 4169-4176.
- [68] J.Y.T. Kim, P. Zhu, F.-Y. Chen, Z.-Y. Wu, D.A. Cullen, H. Wang, Recovering carbon losses in CO₂ electrolysis using a solid electrolyte reactor, *Nat. Catal.* 5 (2022) 288-299.
- [69] M. Ma, E.L. Clark, K.T. Therkildsen, S. Dalsgaard, I. Chorkendorff, B. Seger, Insights into the carbon balance for CO₂ electroreduction on Cu using gas diffusion electrode reactor designs, *Energy Environ. Sci.* 13 (2020) 977-985.

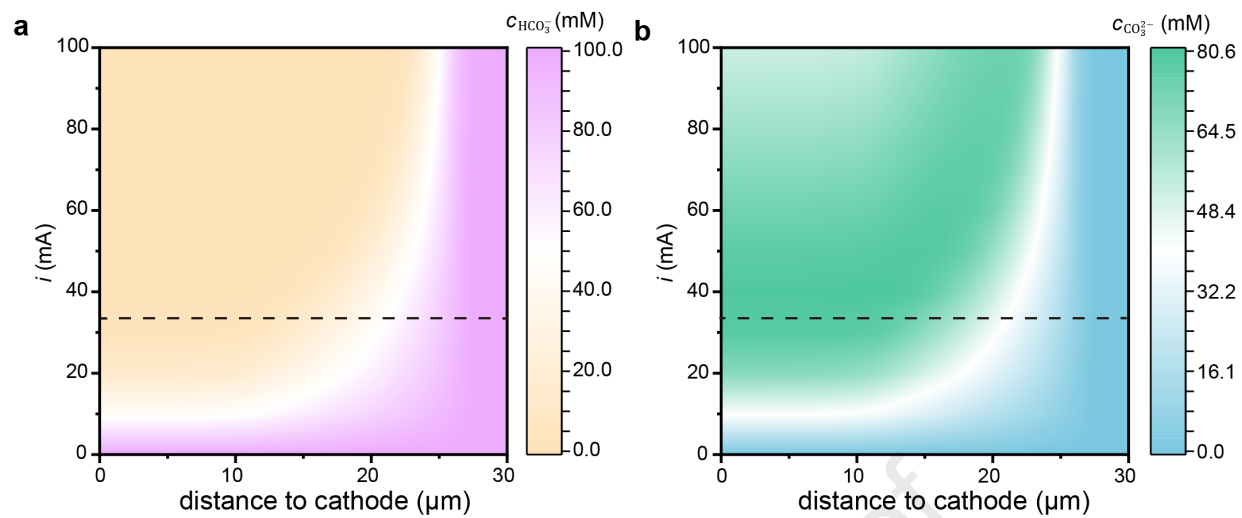


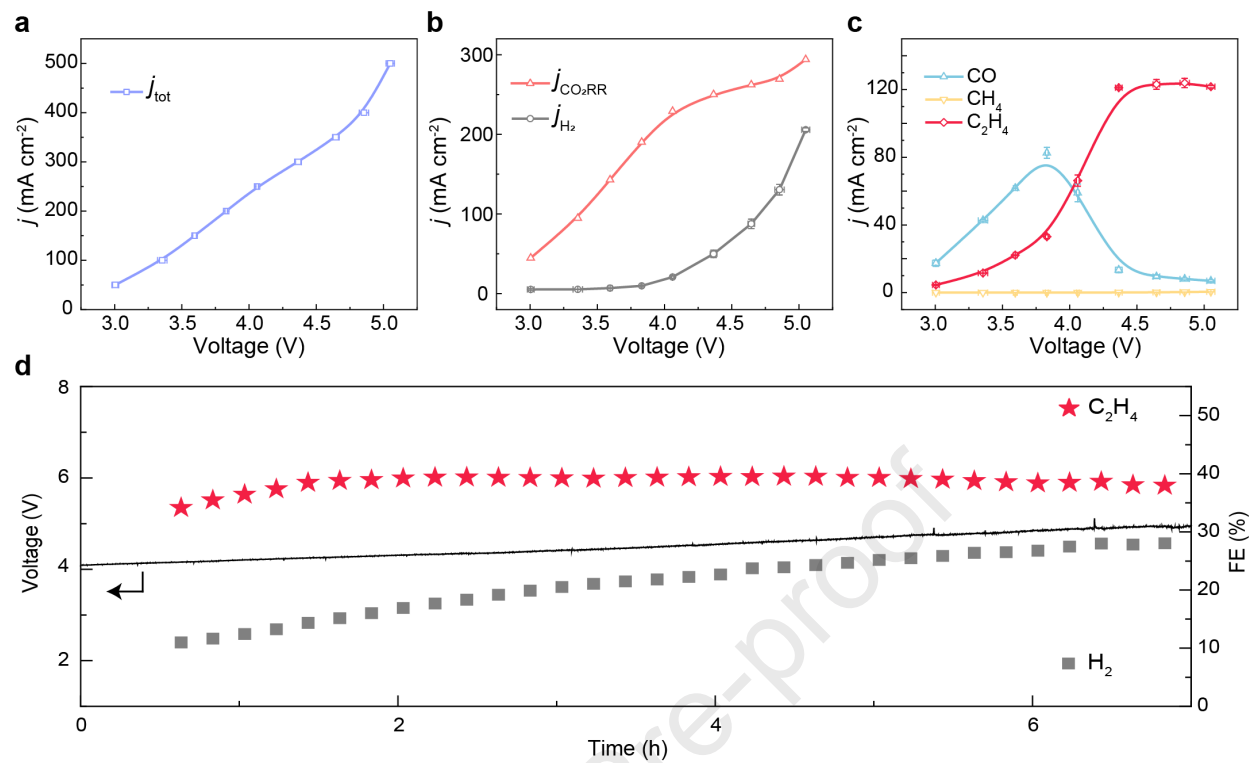












Highlights

- Local reaction environment effects on the CO₂ reduction reaction (CO₂RR) were probed with online differential electrochemical mass spectroscopic (DEMS).
- CO₂ mass transport, local alkalinity, and Cu surface topology led to different CO₂RR pathways.
- Tuning knobs to promote C₂H₄ selectivity were validated on an anion exchange membrane electrolyzer.

Declaration of interests

The authors declare that they have no known competing financial interests or personal relationships that could have appeared to influence the work reported in this paper.

The authors declare the following financial interests/personal relationships which may be considered as potential competing interests:

Journal Pre-proof